J. Fluid Mech. (1970), *vol.* 45, *part* 1, *pp.* 111–130
Printed in Great Britain

On hydromagnetic precession in a cylinder

By ROGER F. GANS

Division of Geological Sciences, California Institute of Technology, Pasadena, California 91109

(Received 3 February 1970 and in revised form 13 July 1970)

The hydrodynamic theory of the resonant cylinder (Gans 1970) is extended to include the effects of a magnetic field parallel to the rotation axis. The linear response is modified by a change in boundary-layer suction and a change in the resonant length. These effects are of equal importance. The theory is valid for small container conductivity and for amplitudes such that the cube of the amplitude is less than the dimensionless precession rate. The importance of container conductivity is assessed. The free modes of the system are given in an appendix. These modes move both east and west.

Experimental apparatus capable of producing magnetic Reynolds numbers of the order of 20 for indefinite lengths of time is described. The apparatus was used to assess the linear theory, though not designed for this purpose. Experiments beyond the range of linear theory are described. The results show finite amplitude effects similar to those previously observed in precessing spheroids in the absence of magnetic effects (Malkus 1968). Additional structure attributable to magnetic effects is observed.

1. Introduction

The only working homogeneous dynamo presently extant is the kinematic dynamo of the Herzenberg type built by Lowes & Wilkinson (1968). The magnetic Reynolds number required to make it operate is of the order of 200. The magnetic Reynolds number in the earth is unknown, but probably lies between 10 and 1000.

Dynamically generated magnetic Reynolds numbers much larger than unity can be attained in precessing systems. In particular, the system described below is felt to attain magnetic Reynolds numbers near 20. These are insufficient for dynamo action in this system; however the existence of the device allows study of these high magnetic Reynolds number flows.

In this paper the problem of a rotating, precessing cylinder of fluid constrained by a magnetic field parallel to the rotation axis is worked in the limit of small precession rate. The theory includes resonance phenomena. (The free modes of the system are given in an appendix.) This work occupies §§ 2–5.

Section 6 describes the experimental apparatus and gives the results of experiments in the range of the theory, as well as extending measurements beyond the range of theory. The experiments agree with theory in the appropriate range. No free dynamo has yet resulted, but the field is amplified by the system.

2. Formulation

Consider a cylindrical container of length L and diameter D, containing an incompressible fluid of density ρ, kinematic viscosity ν, electrical conductivity σ and relative permeability 1. Suppose the cylinder to be rotating about its symmetry axis with angular velocity ω, and that a uniform magnetic field of strength B_0, parallel to the rotation axis, is applied from the outside. Let the entire system precess with angular velocity $\Omega \ll \omega$ about an axis inclined to the symmetry axis with an angle α. For simplicity one can take $\alpha = \frac{1}{2}\pi$, but in principle any α will do.

Steady-state solutions will be sought valid in the multiple limit that

$$E = 4\nu/\omega D^2, \quad E_m = 1/\pi\sigma\omega D^2, \quad C^2 = B_0^2/\pi\omega^2 D^2\rho$$

and

$$R_p = \Omega/\omega$$

are all small. The smallness of the first three parameters allows a boundary-layer treatment, and the fourth parameter provides a linearization.

If $\mathbf{v}$ and $\mathbf{h}$ represent the velocity and magnetic fields, and one non-dimensionalizes according to

$$\mathbf{r} = \tfrac{1}{2}D\mathbf{r}', \quad \mathbf{v} = \tfrac{1}{2}\omega D\mathbf{v}', \quad \mathbf{h} = (B_0/4\pi)\,\mathbf{h}', \quad \boldsymbol{\omega} = \omega\hat{\mathbf{z}}, \quad \boldsymbol{\Omega} = \Omega\hat{\mathbf{x}}; \tag{2.1}$$

the dimensionless equations, in a co-ordinate system rotating with the precession rate, after dropping the primes, are

$$\left.\begin{aligned} \dot{\mathbf{v}} + \mathbf{v}.\nabla\mathbf{v} + 2R_p\,\hat{\mathbf{x}}\times\mathbf{v} + \nabla p - E\nabla^2\mathbf{v} + C^2\mathbf{h}\times\nabla\times\mathbf{h} = 0, \\ \dot{\mathbf{h}} - E_m\nabla^2\mathbf{h} = \nabla\times(\mathbf{v}\times\mathbf{h}) \\ \nabla.\mathbf{v} = 0 = \nabla.\mathbf{h}. \end{aligned}\right\} \tag{2.2}$$

The dimensionless numbers are those defined above, and a co-ordinate system in which the precession direction is $\hat{\mathbf{x}}$ has been chosen.

The boundary conditions for this set are:

$$\left.\begin{aligned} \mathbf{v} = \hat{\mathbf{z}}\times\mathbf{r} \\ \mathbf{n}\times(\mathbf{e},\mathbf{h}) \text{ continuous} \end{aligned}\right\} \quad \text{on} \quad \Sigma,$$

$$\mathbf{h} = \nabla\Phi \to \mathbf{k} \quad \text{as} \quad r\to\infty. \tag{2.3}$$

Here Σ is the container fluid interface, given in a cylindrical co-ordinate system as $\varpi = 1$, $-L/D \leqslant z \leqslant L/D$ and $z = \pm L/D$, $0 \leqslant \varpi \leqslant 1$.

Solutions will be sought using a combined boundary-layer and amplitude expansion, e.g. for the velocity.

$$\mathbf{v} = \mathbf{v}_0 + \epsilon_1\mathbf{v}_1 + \epsilon_2\mathbf{v}_2 + \ldots + \epsilon_1\tilde{\mathbf{v}}_1 + \epsilon_2\tilde{\mathbf{v}}_2 + \ldots, \tag{2.4}$$

where the tilde denotes a boundary-layer quantity, and the ϵ's are functions of E, E_m, C^2, R_p and L/D, with the property $1 \gg \epsilon_1 \gg \epsilon_2$. They will be determined during the course of the analysis. It will be supposed *a priori* that $\epsilon_1 \gg R_p$, by analogy with the viscous resonance in which $\epsilon_1 \sim R_p E^{-\frac{1}{2}}$ and $\epsilon_2 \sim R_p$.

Circumstances for which $\epsilon_1 \sim R_p$ can arise. Such circumstances are analogous to large oblateness in a precessing spheroid in that pressure forces dominate and

the boundary layers do not markedly affect the flow. This case can be obtained from the solution to be derived by taking an appropriate limit.

The zeroth-order solutions are $\mathbf{v}_0 = \hat{\mathbf{z}} \times \mathbf{r}$, $\mathbf{h}_0 = \hat{\mathbf{z}}$ and $\Phi_0 = z$. Since the main thrust of this paper is directed toward understanding the steady-state response, the free modes of the system will be relegated to a brief discussion in the appendix.

The steady parts of the expansion (2.4) are calculated in the following sequence: (1) the zero frequency free mode is found; (2) its boundary layers are calculated; (3) the associated hydromagnetic Ekman suction is calculated; and (4) the amplitude of the zero frequency free mode is calculated by matching the suctions, and departures from resonance, to the precessional force.

3. The first-order interior solution

The equations to $O(\epsilon_1)$ are by definition homogeneous. If solutions proportional to $\exp\{i[st + m\phi]\}$ are sought, one obtains

$$\left.\begin{aligned} i(s+m)\mathbf{v}_1 + 2\hat{\mathbf{z}} \times \mathbf{v}_1 + \nabla V_1 - E\nabla^2 \mathbf{v}_1 - C^2 \partial^2 \mathbf{h}_1/\partial z^2 = 0, \\ i(s+m)\,\mathbf{h}_1 - E_m \nabla^2 \mathbf{h}_1 - \partial \mathbf{v}_1/\partial z = 0, \\ \nabla . \mathbf{v}_1 = 0 = \nabla . \mathbf{h}_1. \end{aligned}\right\} \tag{3.1}$$

The interior equations are obtained from (3.1) by setting $E = E_m = 0$.

The Poincaré force in the precessing co-ordinate system is $2R_p \hat{\mathbf{x}} \times (\hat{\mathbf{z}} \times \mathbf{r})$, and it will excite the solution for which $s = 0$ and $m = 1$. That restriction is imposed here. Other s and m are relegated to the appendix.

Set $s = 0$ and $m = 1$ in (3.1). The second serves to eliminate $\mathbf{h}_1$ in favour of $\mathbf{v}_1$. If u_1, v_1, w_1 are the components of $\mathbf{v}_1$ in cylindrical (ϖ, ϕ, z) co-ordinates, one can eliminate $\mathbf{v}_1$ in favour of V_1 as:

$$\left.\begin{aligned} u_1 &= \frac{-i}{4-\lambda^2}\left[\frac{2}{\varpi} + \lambda \frac{\partial}{\partial \varpi}\right] V_1, \\ v_1 &= \frac{1}{4-\lambda^2}\left[2\frac{\partial}{\partial \varpi} + \frac{\lambda}{\varpi}\right] V_1, \\ w_1 &= \frac{i}{\lambda}\frac{\partial}{\partial z} V_1, \end{aligned}\right\} \tag{3.2}$$

where $\lambda = 1 - \alpha^2 C^2$, where α is the z wave-number. Putting (3.2) into the continuity equation and applying boundary conditions gives the boundary-value problem in V_1,

$$\left.\begin{aligned} \left\{\Delta - \frac{4}{\lambda^2}\frac{\partial^2}{\partial z^2}\right\} V_1 = 0; \\ \left[2 + \lambda \frac{\partial}{\partial \varpi}\right] V_1 = 0 \quad \text{on} \quad \varpi = 1, \\ \frac{\partial}{\partial z} V_1 = 0 \quad \text{on} \quad z = \pm L/D. \end{aligned}\right\} \tag{3.3}$$

This has the solution

$$V_1 = A J_1(k\varpi) \sin \frac{D}{L}\frac{2l+1}{2}\pi z\, e^{i\phi}, \tag{3.4}$$

subject to the two conditions

$$\left.\begin{aligned} k^2 - \left(\frac{2l+1}{2}\pi\frac{D}{L}\right)^2 \frac{4-\lambda^2}{\lambda^2} &= 0, \\ 2J_1(k) + k\lambda J_1'(k) &= 0. \end{aligned}\right\} \tag{3.5}$$

These form a coupled transcendental set to determine k and L/D, and solutions exist only for discrete values of L/D. For $\lambda = 1$, the hydrodynamic case, these solutions are known, and for any L/D one can come arbitrarily close to solving (3.5) by the appropriate choice of k and l. In physical systems arbitrarily close is close enough and one can consider (3.5) satisfied. The solution of (3.5) represents a resonance, and the aim of this paper is to discuss this resonance, and the behaviour of the fluid in the immediate vicinity of the resonance. In principle one must calculate all resonances. This is not necessary in practice. The resonant amplitude is known for $\lambda = 1$ (Gans 1970). For this case the resonant amplitude goes like $l^{-\frac{1}{2}}$ for large l. It is thus less than the non-resonant amplitude, which is $O(R_p)$, for sufficiently large l. One can make this clearer as follows. Let l_r be the wave-number for which (3.5) is satisfied for some particular L/D and $C^2 = 0$. The generalized pressure V is then given by

$$V = \epsilon A(l_r)\Psi_{l_r}(\varpi, \phi, z) + \sum_{l \neq l_r} R_p A_l \Psi_l(\varpi, \phi, z), \tag{3.6}$$

where $\Psi(\varpi, \phi, z)$ are normalized eigenfunctions satisfying the first two of (3.3). For sufficiently large l_r

$$\epsilon_1 A(l_r) < R_p. \tag{3.7}$$

In the event that (3.7) holds, the solution will be called non-resonant; otherwise the solution will be called resonant. For $C^2 = 0$, $L/D = 1$ corresponds to $l = 1$, and is the principal resonance. Potential resonances in the vicinity of $L/D = 1$ have amplitudes satisfying (3.7), and so by varying L/D in the neighbourhood of 1, the smooth change between resonant and non-resonant configurations can be exhibited. The assumption that this holds for small but non-zero C^2 as well provides a motivation for the modification of k and α to be described. The usual procedure of modifying the frequency, s, is unsuitable here, because the choice $s = 0$ is fixed by the choice of co-ordinate system.

The nearly resonant problem near $L/D = 1$ can be described as follows. Let $k = \frac{1}{2}\sqrt{3}\pi + k_1$, $\alpha = \frac{1}{2}\pi + \alpha_1$ and $L/D = 1 + f$. Here k_1, α_1 and f are all supposed to be small quantities, such that their products with ϵ_1 can be considered to be of second order. Equations (3.3) then reduce to

$$\left.\begin{aligned} -\sqrt{3}\pi k_1 + 3\pi\alpha_1 + \pi^4 C^2 &= 0, \\ 3(1 + \tfrac{1}{4}\pi^2)k_1 &= \sqrt{3}\,\tfrac{1}{4}\pi^3 C^2, \\ \cos\alpha(1+f) &= 0. \end{aligned}\right\} \tag{3.8}$$

From the first two one obtains

$$\left.\begin{aligned} k_1 &= \frac{\sqrt{3}\,\pi^3}{12 + 3\pi^2} C^2, \\ \alpha_1 &= -\frac{\pi^3}{6}\frac{2+\pi^2}{4+\pi^2} C^2, \end{aligned}\right\} \tag{3.9}$$

which are small for C^2 small. The third equation introduces a term like Ekman suction, of $O[\max(f, C^2)]$, which can be considered at the same time as Ekman suction. This approach is the same conceptually as that used by Busse in considering the response to precession of an oblate spheroid (Busse 1968), considered to first order to be a sphere. The added complication of an 'effective oblateness' which is a function of C^2 should not be allowed to obscure this point. As will become apparent in the boundary-layer analysis there is a strong analogy between cylinders with an aspect ratio near unity and spheroids of small oblateness.

There remains the normal boundary condition on the magnetic field. A complete discussion requires consideration of the conductivity of the container and the nature of the fields in the container. To that end let the conductivity of the container be $S\sigma$, and suppose the end plates to have thickness d. Magnetic boundary conditions on the sidewalls are of less importance, as will become clear later.

The magnetic field in the end plates, $\epsilon_1 \mathbf{h}^E$, satisfies

$$\left(\frac{\partial}{\partial\phi} - \frac{E_m}{S}\nabla^2\right)\mathbf{h}^E = 0, \tag{3.10}$$

and the usual decomposition

$$\mathbf{h}^E = \nabla\times(\mathbf{k}\Psi^T) + \nabla\times\nabla\times(\mathbf{k}\Psi^P), \tag{3.11}$$

can be used to simplify the representation. Here Ψ^T and Ψ^P are the toroidal and poloidal defining scalars and they satisfy the scalar equivalent of (3.10),

$$\left(\frac{\partial}{\partial\phi} - \frac{E_m}{S}\Delta\right)(\Psi^T, \Psi^P) = 0. \tag{3.12}$$

The condition that the tangential components of the electric field be continuous across the boundary can be divided into two conditions, one involving Ψ^P only and the other Ψ^T only. The former represents the continuity of normal component of $\mathbf{B}$, and the latter is a construct related to the gradient of current. Formally these are obtained by taking the sum and difference of the electric field conditions. For no-slip velocity conditions these are finally

$$\left.\begin{aligned} \hat{\mathbf{z}}.\mathbf{h} &= \Psi^P_{,zz} - \frac{iS}{E_m}\Psi^P, \\ S\left\{\frac{1}{\varpi}\frac{\partial}{\partial\varpi}[\varpi\hat{\boldsymbol{\phi}}.(\nabla\times\mathbf{h})] + \frac{1}{\varpi}\frac{\partial}{\partial\phi}[\hat{\boldsymbol{\varpi}}.(\nabla\times\mathbf{h})]\right\} &= \frac{2}{\varpi}\Psi^T_{,z\varpi\phi}. \end{aligned}\right\} \tag{3.13}$$

The comma-subscript notation will be used to denote differentiation of the defining scalars.

At $z = \pm(L+d)/D$ the end plate field must be fitted to an exterior potential. If this potential is denoted by Φ, the boundary conditions are

$$k^2\Psi^P = \Phi_{,z}, \quad \Psi^P_{,z} = \Phi, \quad \Psi^T = 0. \tag{3.14}$$

Locally $\Phi \propto e^{-kz} J_1(k\varpi)\, e^{i\phi}$, and the boundary conditions determine Ψ^P as

$$\Psi^P = (\hat{\mathbf{z}}.\mathbf{h})_{z=\pm L/D} \operatorname{csch}\mu \frac{d}{D}\left\{\frac{\mu \operatorname{csch}\mu d/D}{k^2\mu\coth\mu d/D + k^3}\sinh\mu\left(z \mp \frac{d}{D}\right) - \frac{1}{k^2}\sinh\mu\left(z \mp \frac{L+d}{D}\right)\right\}. \quad (3.15)$$

Here $\mu^2 = k^2 + iS/E_m$.

The tangential fields associated with Ψ^P are given by the gradient of $\Psi^P_{,z}$. By expanding in powers of $\mu d/D$ one can show that

$$\Psi^P_{,z} = -\frac{\hat{\mathbf{z}}.\mathbf{h}}{k}\operatorname{sech}^2\mu \frac{d}{D}\left[1 + O\left(\mu\frac{d}{D}\right)\right], \quad (3.16)$$

for small $\mu d/D$ and so is bounded as $\mu d/D \to 0$.

Before proceeding to the boundary-layer formulation, the tangential boundary values will be derived. On $z = \pm L/D$

$$\left.\begin{aligned} u_1 &= \frac{\pm iA}{\lambda^2-4}\left[\frac{2}{\varpi} + \lambda\frac{\partial}{\partial\varpi}\right] J_1(k\varpi)\, e^{i\phi}, \\ v_1 &= \frac{\mp A}{\lambda^2-4}\left[2\frac{\partial}{\partial\varpi} + \frac{\lambda}{\varpi}\right] J_1(k\varpi)\, e^{i\phi}, \\ h_{1\varpi} &= 0 = h_{1\phi}, \end{aligned}\right\} \quad (3.17)$$

and on $\varpi = 1$,

$$\left.\begin{aligned} v_1 &= \frac{-A}{\lambda^2-4}\{2kJ_1'(k) + \lambda J_1(k)\}\sin\frac{2n+1}{2}\pi\frac{D}{L}z\, e^{i\phi}, \\ w_1 &= iA\frac{2n+1}{2}\pi\frac{D}{L}J_1(k)\cos\frac{2n+1}{2}\pi\frac{D}{L}z\, e^{i\phi}, \\ h_{1\phi} &= \frac{iA}{\lambda^2-4}\frac{2n+1}{2}\pi\frac{D}{L}\{2kJ_1'(k) + \lambda J_1(k)\}\cos\frac{2n+1}{2}\pi\frac{D}{L}z\, e^{i\phi}, \\ h_{1z} &= -A\left[\frac{2n+1}{2}\pi\frac{D}{L}\right]^2 J_1(k)\sin\frac{2n+1}{2}\pi\frac{D}{L}z\, e^{i\phi}. \end{aligned}\right\} \quad (3.18)$$

4. The boundary layers

The form of the boundary layers will be different on the flat caps of the cylinder from the form on the curved sidewalls. The caps will be discussed first.

On the upper cap, $z = L/D$, let the boundary-layer dependent variables be proportional to

$$\exp\left[-\delta^{-1}\left(\frac{L}{D} - z\right) + i\phi\right]. \quad (4.1)$$

The 'boundary-layer thickness' is δ, supposed to be small compared to one, and required to have positive real part. The boundary-layer equations are then

$$\left.\begin{aligned} (i - E\,\delta^{-2})(\tilde{u}_1, \tilde{v}_1, \tilde{w}_1) + 2(-\tilde{v}_1, \tilde{u}_1, 0) + (\tilde{V}_{1,\varpi}, \varpi^{-1}\tilde{V}_{1,\phi}, \tilde{V}_{1,z}) &= -C^2\delta^{-1}\tilde{\mathbf{h}}_1, \\ (i - E_m\delta^{-2})\tilde{\mathbf{h}}_1 = \delta^{-1}\tilde{\mathbf{v}}_1, \quad \tilde{w}_1 = 0 = \tilde{h}_{1z}. & \end{aligned}\right\} \quad (4.2)$$

The two divergence conditions require the z components of $\tilde{\mathbf{v}}_1$ and $\tilde{\mathbf{h}}_1$ to be zero and the z component of the momentum equation requires $\tilde{V}_1$ to be zero. The

magnetic diffusion equation can be used to eliminate $\tilde{\mathbf{h}}_1$ in favour of $\tilde{\mathbf{v}}_1$, and the tangential components of the momentum equation form the reduced boundary-layer equations:

$$\{(i-E\delta^{-2})(i-E_m\delta^{-2})+C^2\delta^{-2}\}(\tilde{u}_1,\tilde{v}_1)+2(i-E_m\delta^{-2})(-\tilde{v}_1,\tilde{u}_1)=0. \quad (4.3)$$

The term in C^2 arises from the fluid-container coupling caused by the penetration of the field lines through the container wall. The characteristic equation for δ is

$$(i-E\delta^{-2})(i-E_m\delta^{-2})+C^2\delta^{-2}=\pm 2i(i-E_m\delta^{-2}). \quad (4.4)$$

For $C^2=0$ this leads to the usual Ekman layer. For non-zero C^2 this can be solved exactly to give for δ

$$\left.\begin{aligned}\delta^2 &= -\frac{1}{2}\left\{\frac{iE}{1\mp 2}-\frac{C^2}{1\mp 2}+iE_m\right\},\\ (\pm)\frac{1}{2}&\sqrt{\left[\left\{\frac{iE}{1\mp 2}-\frac{C^2}{1\mp 2}+iE_m\right\}^2+\frac{4EE_m}{1\mp 2}\right]}.\end{aligned}\right\} \quad (4.5)$$

The $\pm$ in parentheses is independent of that in front of the 2's. In liquid metals $E \ll E_m$ and one can expand the radical in powers of E. Doing this gives the approximate representations for the boundary-layer parameters:

$$\left.\begin{aligned}\delta^2 &\approx -\frac{iEE_m}{E_m(1\mp 2)+iC^2}, \quad \text{viscous},\\ \delta^2 &\approx -iE_m+\frac{C^2}{1\mp 2}+\frac{EC^2}{(1\mp 2)[E_m(1\mp 2)+iC^2]}, \quad \text{magnetic}.\end{aligned}\right\} \quad (4.6)$$

The viscous layer reduces to the Ekman layer when $C^2\to 0$. The magnetic boundary layer grows to fill the entire volume as $C^2\to 1$; the boundary-layer technique does not work for $C^2 \geqslant 1$. For $C^2 \gg E_m$, the viscous layer is purely imaginary at the lowest order and appears not to decay. A further analysis shows an effective decay rate of $(E_m/E)^{\frac{1}{2}}C^{-1} \gg 1$ so the boundary-layer approximation remains valid.

The viscous boundary-layer parameters will be assigned subscripts 1 and 2 and the magnetic parameters 3 and 4. The boundary-layer velocities and fields are then written

$$\left.\begin{aligned}\tilde{u}_1 &= \sum_{p=1}^{4} A_p \exp\{(z-L/D)/\delta_p+i\phi\},\\ \tilde{v}_1 &= \Sigma i(-)^p A_p \exp\{(z-L/D)/\delta p+i\phi\},\\ \tilde{h}_{1\varpi} &= \Sigma L_p A_p \exp\{(z-L/D)/\delta p+i\phi\},\\ \tilde{h}_{1\phi} &= \Sigma i(-)^p L_p A_p \exp\{(z-L/D)/\delta p+i\phi\},\end{aligned}\right\} \quad (4.7)$$

where L_p comes from equation (4.2), and is

$$L_p = \delta_p(i\delta_p^2-E_m)^{-1}.$$

For p even one takes the upper sign in (4.6), and for p odd, the lower.

Application of the boundary conditions to (4.7) is a two-step process if the conductivity of the end plate is to be included. The toroidal field in the end plate must be assessed. One begins with the four boundary conditions

$$\left.\begin{aligned} u_1+\tilde{u}_1 &= 0,\\ v_1+\tilde{v}_1 &= 0,\\ \tilde{h}_{1\varpi} &= \Psi^P_{,z\varpi}+(i/\varpi)\,\Psi^T,\\ \tilde{h}_{1\phi} &= (i/\varpi)\,\Psi^P_{,z}-\Psi^T_{,\varpi}, \end{aligned}\right\} \tag{4.8}$$

where Ψ^T is the toroidal defining scalar introduced in § 3. These are used to eliminate the A_p in favour of the boundary values of Ψ^T. The fifth boundary condition is the boundary-layer equivalent of the second of (3.13), viz.

$$-S\nabla.\left(\frac{\partial\tilde{\mathbf{h}}_1}{\partial z}\right)=\frac{2i}{\varpi}\Psi^T_{,z\varpi}. \tag{4.9}$$

The A_p are given by

$$\left.\begin{aligned} e^{i\phi}A_1 &= -\frac{1}{2}\frac{L_3}{L_3-L_1}(u_1+iv_1)^b-\frac{1}{2}\frac{1}{L_3-L_1}\left\{\Psi^P_{,z\varpi}-\frac{1}{\varpi}\Psi^P_{,z}+\frac{i}{\varpi}\Psi^T+i\Psi^T_{,\varpi}\right\}^b,\\ e^{i\phi}A_2 &= -\frac{1}{2}\frac{L_4}{L_4-L_2}(u_1-iv_1)^b-\frac{1}{2}\frac{1}{L_4-L_2}\left\{\Psi^P_{,z\varpi}+\frac{1}{\varpi}\Psi^P_{,z}+\frac{i}{\varpi}\Psi^T-i\Psi^T_{,\varpi}\right\}^b, \end{aligned}\right\} \tag{4.10}$$

where the superscript b denotes evaluation at the boundary. A_3 and A_4 are obtained from A_1 and A_2 by interchanging L_1 and L_3 and L_2 and L_4, respectively.

The divergence of $\partial\tilde{\mathbf{h}}_1/\partial z$ is given by

$$\sum_{p=1}^{4}\frac{L_p}{\delta_p}\left\{\frac{1}{\varpi}\frac{\partial}{\partial\varpi}(\varpi A_p)\,(-)^{p+1}\frac{1}{\varpi}A_p\right\}. \tag{4.11}$$

This can be written as

$$\begin{aligned} \nabla.\left(\frac{\partial\tilde{\mathbf{h}}_1}{\partial z}\right) &= \tfrac{1}{2}ik^2V_1^b\left\{\frac{3}{i\delta_2\,\delta_4+E_m}-\frac{1}{i\delta_1\,\delta_3+E_m}\right\}\\ &\quad+\tfrac{1}{2}k^2(\Psi^P_{,z})^b\left\{\frac{i(\delta_1+\delta_3)}{i\delta_1\,\delta_3+E_m}+\frac{i(\delta_2+\delta_4)}{i\delta_2\,\delta_4+E_m}\right\}\\ &\quad-\frac{1}{2}\frac{\delta_1+\delta_3}{i\delta_1\,\delta_3+E_m}\left\{\Psi^T_{,\varpi\varpi}+\frac{3}{\varpi}\Psi^T_{,\varpi}+\frac{1}{\varpi^2}\Psi^T\right\}^b\\ &\quad+\frac{1}{2}\frac{\delta_2+\delta_4}{i\delta_2\,\delta_4+E_m}\left\{\Psi^T_{,\varpi\varpi}-\frac{1}{\varpi}\Psi^T_{,\varpi}+\frac{1}{\varpi^2}\Psi^T\right\}^b, \end{aligned} \tag{4.12}$$

after some algebraic manipulation. The constants on the right-hand side have the respective orders E_m^{-1}, $E_m^{-\frac{1}{2}}$, $E_m^{-\frac{1}{2}}$ and $E_m^{-\frac{1}{2}}$. The dominant term is thus the first. This (times S) is to be balanced against the right-hand side of (4.9), which is $\sim(D/d)\Psi^T$. Hence

$$\Psi^T\sim\frac{Sd}{E_mD}. \tag{4.13}$$

The scaling rule (4.13) is not the obvious scaling one might expect from inspection of (4.9). That brief inspection would give $\Psi^T\sim Sd/D\delta$, where δ is the boundary-layer thickness. Such an estimate would be correct in simpler

hydromagnetic problems where there is only one boundary-layer scale. Examples are Hartmann flow, Hartmann flow with rotation and some axisymmetric problems. It is the lack of axisymmetry which gives rise to two boundary-layer scales which are not totally separated. Uncoupled double scales occur in this problem on the sidewalls where the rotation vector is parallel to the boundary. What the coupled boundary layers mean physically is that the magnetic field changes in the viscous boundary layer by $O(E^{\frac{1}{2}}E_m^{-1})$, so that one obtains

$$\Psi^T \sim \frac{Sd}{D}\frac{E^{\frac{1}{2}}}{E_m \delta_{\text{viscous}}} \sim \frac{Sd}{E_m D},$$

rather than

$$\Psi^T \sim \frac{Sd}{D}\frac{1}{\delta_{\text{magnetic}}}.$$

In what follows $Sd/E_m D$ will be supposed small so that the toroidal field need not be explicitly considered.

The sidewall layers are simpler because the zeroth-order field does not penetrate the sidewalls. Using the magnetic diffusion equation to eliminate $\tilde{\mathbf{h}}_1$, and the divergence condition to force $\tilde{u}_1$ to be zero leads to the characteristic equation for the boundary-layer parameter δ

$$i - E\delta^{-2} - \frac{C^2\delta^2}{i\delta^2 - E_m}\left(\frac{2n+1}{2}\pi\frac{D}{L}\right)^2 = 0. \tag{4.14}$$

This quadratic in δ^2 can be solved exactly. The result separates into

$$\left.\begin{aligned} \delta^2 &\approx -\frac{iE}{1-C^2\alpha^2}(1+C^2\alpha^2), \quad \text{viscous,} \\ \delta^2 &\approx -\frac{iE_m}{1-C^2\alpha^2} + \frac{EC^2\alpha^2}{1-C^2\alpha^2}, \quad \text{magnetic,} \end{aligned}\right\} \tag{4.15}$$

and these are essentially independent of C^2 for $C^2 \ll 1$, and they are the boundary layers one would obtain by treating the momentum and diffusion equations separately. These two different types of boundary layers illustrate quite clearly the difference between strong-coupling caused by a poloidal-type field, and the weak coupling caused by a toroidal-type field.

Let δ_v represent the viscous boundary layer and δ_m the magnetic. Substituting into the boundary conditions

$$\left.\begin{aligned} v_1 + \tilde{v}_1 &= 0, \\ w_1 + \tilde{w}_1 &= 0, \\ h_{1\phi} + \tilde{h}_{1\phi} &= (i/\varpi)\,\Phi_1, \\ h_{1z} + \tilde{h}_{1z} &= (\partial/\partial z)\,\Phi_1, \end{aligned}\right\} \tag{4.16}$$

gives the boundary-layer variables

$$\left.\begin{aligned} \tilde{v}_1 &= -v_1|_{\varpi=1}\, e^{(\varpi-1)/\delta_v}, \\ \tilde{w}_1 &= -w_1|_{\varpi=1}\, e^{(\varpi-1)/\delta_v}, \\ \tilde{h}_{1\phi} &= \left[i\frac{\partial v_1}{\partial z} + \frac{i}{\varpi}\Phi\right]_{\varpi=1} e^{(\varpi-1)/\delta_m}, \\ \tilde{h}_{1z} &= \left[i\frac{\partial w_1}{\partial z} + \Phi_{,z}\right]_{\varpi=1} e^{(\phi-1)/\delta_m}. \end{aligned}\right\} \tag{4.17}$$

The divergences of $\tilde{\mathbf{v}}_1$ and $\tilde{\mathbf{h}}_1$ do not vanish, but produce the hydromagnetic analogue of Ekman suction. The magnetic divergence is matched by a second-order exterior potential, but the velocity divergence can only be matched by a second-order interior velocity field, as is the usual situation in problems of this nature. This velocity divergence joins the divergence associated with the 'effective oblateness' as defined in the previous section in the second-order interior boundary conditions. The divergences of (4.7) and (4.17) are

$$\left.\begin{aligned} \epsilon_2 \tilde{w}_2 &= -\epsilon_1 \sum_p \left\{ \frac{1}{\varpi} \frac{\partial}{\partial \varpi} (\varpi \delta_p A_p)(-)^{p+1} \frac{1}{\varpi} \delta_p A_p \right\}; \\ \epsilon_2 \tilde{u}_2 &= \epsilon_1 \delta_v \left\{ \frac{i}{\varpi} v_1 + \frac{\partial w_1}{\partial z} \right\}_{\varpi=1}. \end{aligned}\right\} \tag{4.18}$$

5. The second-order problem

The second-order interior fields satisfy inhomogeneous equations of the form of (3.1) with inhomogeneous boundary conditions. The sequence of operations leading to (3.3) produce the equations

$$\left.\begin{aligned} &\left[\Delta - \frac{4}{\lambda_2} \frac{\partial^2}{\partial z^2}\right] V_2 = 0, \\ &\left[2 + \lambda \frac{\partial}{\partial \varpi}\right] V_2 = i(\lambda^2 - 4)\, \tilde{u}_2 \quad \text{on} \quad \varpi = 1, \\ &\frac{\partial V_2}{\partial z} = i\lambda \left[\tilde{w}_2 + \frac{\epsilon_1}{\epsilon_2} w_1\right] + 2 \frac{R_p}{\epsilon_2} \varpi e^{i\phi} \quad \text{on} \quad z = \pm L/D. \end{aligned}\right\} \tag{5.1}$$

Rewriting the equations in terms of V_2 has moved the forcing term into the boundary conditions. The oblateness term has been denoted by w_1.

The function

$$\Psi = J_1(k\varpi) \sin \alpha z\, e^{i\phi}$$

satisfies the homogeneous equivalent of (5.1) for the correct values of k and α. This homogeneous equivalent is (3.3), and V_1 is proportional to Ψ. In order that (5.1) have a solution, then, the inhomogeneous terms must be orthogonal to Ψ. The condition that this be true is obtained by multiplying the first of (5.1) by Ψ^* and integrating over the volume. Integrating by parts and making use of the boundary conditions gives the solvability condition in terms of the surface integrals

$$\begin{aligned} 0 = \int_{\varpi=1} \Psi^* i(\lambda^2 - 4)\, \tilde{u}_2\, dS - 6 \int_{z=L/D} \Psi^* i\lambda \left(\tilde{w}_2 + \frac{\epsilon_2}{\epsilon_1} w_1\right) dS \\ - 12 \frac{R_p}{\epsilon_2} \int_{z=L/D} \Psi^* \varpi\, e^{i\phi}\, dS. \end{aligned} \tag{5.2}$$

The symmetry properties of V_1, V_2 and Ψ have been used to eliminate the integrals over $z = -L/D$ in terms of those over $z = L/D$.

From equation (3.2), w_1 is given by

$$w_1|_{z=L/D} = -\tfrac{1}{2} i\pi \sin(\tfrac{1}{2}\pi f - \alpha_1)\, A_1 J_1(\tfrac{1}{2}\sqrt{3}\pi\varpi)\, e^{i\phi}, \tag{5.3}$$

where A_1 is the (as-yet-undetermined) amplitude of V_1 and the specific situation $L/D = 1+f$ has been taken. From (4.7) $\epsilon_2 \tilde{w}_2$ can be written

$$\epsilon_2 \tilde{w}_2 = -\frac{ik^2}{6}\left[\frac{\delta_1 L_3 - \delta_3 L_1}{L_3 - L_1} - 3\frac{\delta_2 L_4 - \delta_4 L_2}{L_4 - L_2}\right]\epsilon_1 A_1 J_1(\tfrac{1}{2}\sqrt{3}\pi\varpi)\, e^{i\phi} - \frac{1}{2}\left[\frac{\delta_1 - \delta_3}{L_3 - L_1} + \frac{\delta_2 - \delta_4}{L_4 - L_2}\right] k^2 \Psi^P_{,z}|_{z=1}. \quad (5.4)$$

The second of (4.18) gives

$$i\epsilon_2 \tilde{u}_2 = [(1-i)\sqrt{2}]\, E^{\frac{1}{2}}(1+\tfrac{1}{4}\pi^2)\,\epsilon_1 A_1 J_1(\tfrac{1}{2}\sqrt{3}\pi)\sin\tfrac{1}{2}\pi z\, e^{i\phi}. \quad (5.5)$$

An algebraic equation for $\epsilon_1 A_1$ is obtained by substituting (5.3), (5.4), and (5.5) into (5.2) and performing the integrations. The Bessel function integrals can be found in Erdelyi *et al.* (1953, equations (7.1) (1) and (7.10)(49)). After some algebraic manipulation (5.2) becomes

$$\epsilon_1 A_1 \left\{\sqrt{2}(1-i)E^{\frac{1}{2}} + \frac{\sqrt{(EE_m)}\,(\delta_1+\delta_3)}{E_m\sqrt{3}+\sqrt{(EE_m)}} - 3i\frac{\sqrt{(EE_m)}\,(\delta_2+\delta_4)}{E_m + i\sqrt{(EE_m)}} + F\left(\mu\frac{d}{D}\right)\frac{\sqrt{3}\pi}{2}\frac{2E_m - (\sqrt{3}+i)\sqrt{(EE_m)}}{3E_m + (3i-\sqrt{3})\sqrt{(EE_m)} - iE} + \frac{4}{\pi}\sin\left[\frac{\pi}{2}f - \frac{\pi^3}{6}\frac{2+\pi^2}{4+\pi^2}C^2\right]\right\} = -\frac{128R_p}{\pi^2(\pi^2+4)\,J_1(\frac{1}{2}\sqrt{3}\pi)}. \quad (5.6)$$

The amplitude $A_1\epsilon_1$ is limited by the terms in the wavy bracket on the left-hand side. These are of four types. The first term represents viscous divergence on the sidewalls. The second and third terms represent viscous divergence on the end plates. The fourth term represents the modification of the velocity divergence caused by the bending of field lines in the boundary layer and the fifth term represents the pressure forces arising from the effective oblateness. If $f \sim 1$ this term dominates and one obtains the leading term of the non-resonant expansion of V_2, as expressed in (3.6).

The term $F(\mu d/D) \to 1$ as $\mu(d/D) \to 0$. It is otherwise complex, so that the expression (5.7) is not singular for $E = 0, \mu \neq 0$. Physically this represents a drag on the magnetic field lies by the conducting boundaries so that relative motion between the fluid and the container wall is limited in the absence of viscosity when a magnetic field is present.

For the purpose of evaluating (5.7) this effect is not important. For calculation $F(\mu d/D)$ is set equal to unity and the δ_p are replaced by their approximate representations (4.6), and only the leading terms in each expression is retained, leading to

$$\epsilon_1 A_1 = -\frac{128\sqrt{6}\,R_p}{\pi^2(\pi^2+4)\,J_1(\frac{1}{2}\sqrt{3}\pi)}\frac{2\sqrt{6}f - (\sqrt{3}-1)E^{\frac{1}{2}} + BC^2 + (5\sqrt{3}+1)iE^{\frac{1}{2}}}{\{[2\sqrt{6}f - (\sqrt{3}-1)E^{\frac{1}{2}} + BC^2]^2 + (5\sqrt{3}+1)^2 E\}}, \quad (5.7)$$

where

$$B = \sqrt{2}\,\pi\left[1 - \frac{2\pi}{\sqrt{3}}\frac{2+\pi^2}{4+\pi^2}\right].$$

For $C^2 = f = 0$ this reduces to the hydrodynamic results (Gans 1970). Note that B is negative, so that the effect of the magnetic field is to reduce the effective length of the container. For positive f there is a maximum in the function $A_1\epsilon_1(C^2)$. This is not true for negative f, corresponding to an 'oblate' cylinder.

The analysis leading to this result has neglected non-linear terms of order ϵ_1^2. These are automatically orthogonal to ψ and cannot affect the analysis. The non-linear terms are first important at order ϵ_1^3. The precession rate limit is then derived from the *constant* that

$$\epsilon_1^3 < R_p.$$

From (5.8) one obtains $$R_p < \max\{f^{*\frac{3}{2}}, E^{\frac{3}{4}}, C^2\} \tag{5.8}$$

as the condition under which the linear theory can be expected to hold. Here

$$f^* = f - (2/\pi)\alpha_1,$$

is the 'effective oblateness'.

6. Discussion and experiment

By taking advantage of the strong responses of rotating fluids to precession, it is possible to build a practical device which can sustain magnetic Reynolds numbers of the order of 20 indefinitely. The first such device successfully built is described below. Because of the stringent nature of the linearity condition (5.9), the device is not well-suited to test the theory, requiring very slow precession rates to maintain a linear response, even for f significantly different from zero. A second problem is the question of toroidal fields in the end plates. The estimate (4.13), using $S \sim \frac{1}{8}$, $d/D \sim \frac{1}{25}$ and $E_m \sim \frac{1}{75}$, gives $\psi^T \sim \frac{3}{8}$, which is not negligible. This, however, is an upper bound. First, any degradation of the surface by the molten sodium would reduce the effective S. The second reduction arises from the fact that ψ^T, and the contributions to the suction arising from ψ^T, are in part orthogonal to the integrating function used in (5.2), so that they do not contribute in full strength. These two effects supply the rationale for attempting to compare the experimental results with the theory. That this attempt is successful indicates that the rationale is valid. (Note that this effect enters the coefficient multiplying C^2, whereas f is a constant independent of C^2. This conductivity argument is different from the later discussion regarding f. The results are not an example of compensating errors.)

The real value, and the purpose, of the experiment is not the illumination of the linear theory, but exploration of possible high magnetic Reynolds number effects, in particular possible modifications of hysteresis effects observed in non-conducting fluids in spheroids (Malkus 1968) and cylinders (Gans 1969). The results reported here are in a sense preliminary, but the experiment is sufficiently novel to warrant reporting at this time.

The device in question is basically a stainless steel cylinder 25 cm in diameter, filled with liquid sodium, which can be rotated about its symmetry axis at angular velocities up to 3600 rev/min, and precessed about an axis at right angles to the symmetry axis at angular velocities up to 50 rev/min. Co-axial with the cylinder is a d.c. coil used to apply an axisymmetric field to the sodium. The container and coil are mounted on a rotating table driven by a variable speed electric transmission and floating on air bearings.

The details of construction of the cylinder are as shown in figure 1. The initial filling is conducted through port A. During this filling nitrogen is allowed to leak slowly through the system to minimize oxidation of the sodium. Before filling the entire system is thoroughly flushed with nitrogen. The valve B was held open during the filling operation, which took several minutes. After filling the port A was closed and the container spun up to 2400 rev/min. At this point operations could be stopped by allowing the sodium to freeze while the container continued to spin, and this is the usual shut-down procedure. Since the sodium freezes under centrifugal force, this leaves a central core and allows access to the valve B and its controls.

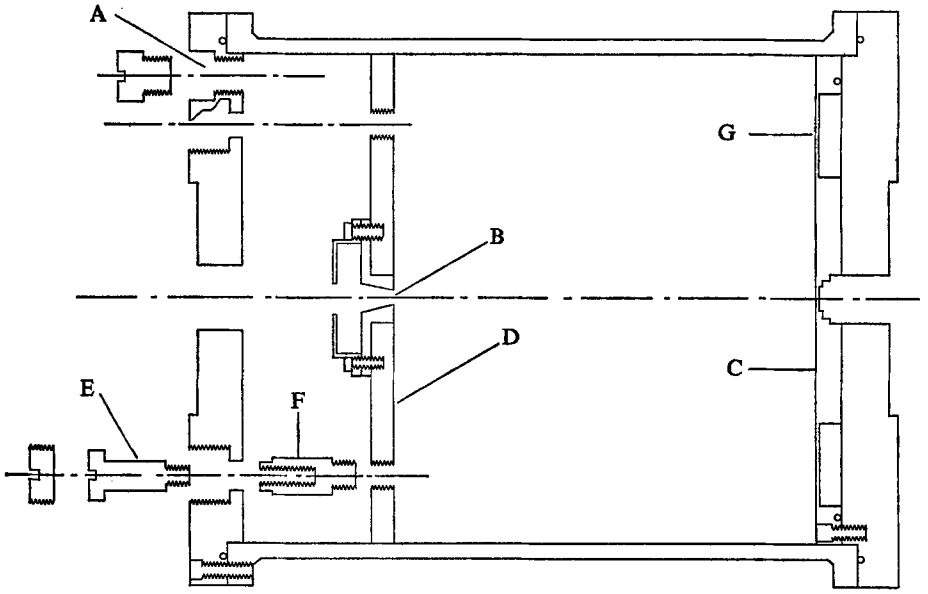

FIGURE 1. Schematic section of the hydromagnetic cylinder.

The sequence followed to prepare the device for an experiment is as follows. The device is spun-up cold and a small nitrogen pressure maintained. An insulated box is put over the cylinder and the field coils. A current of 10 amps is passed through the field coil, heating the air space around the cylinder and melting the sodium in about half an hour. During the melting period the temperature of the sodium is monitored with the thermocouple C. A thermocouple wound into the field coils monitors their temperature and a dial thermometer fitted into a hole in the insulated box monitors the air temperature. After melting the temperature is allowed to rise from the melting point of 98 °C, to 115 °C.

At this point there is a nitrogen core passing through the entire device. To remove this the phenomenon of differential spin-up is utilized. The motor driving the cylinder is turned off and the system allowed to slow down to 1000 rev/min. Then the container is spun up 'impulsively' to its full rotation rate of 2400 or 3600 rev/min. This takes less than a second. The fluid behind the baffle spins up much more rapidly than the fluid in the test section, creating a differential centrifugal pressure driving fluid into the test section and gas, through the

valve B, out of the section. This is done twice, with an overpressure of 2–3 atmospheres of nitrogen to prevent the formation of a vacuum core.

The actual valve used in this device was tested in a plastic cylinder filled with water. It was only 15 cm in diameter and rotated at 1800 rev/min so the forces were much smaller. This procedure cleared essentially all of an air core from the test section in two repetitions. No method has yet been devised to measure whether or not the system works in the sodium.

The position of the baffle D, which controls the length of the test section, is adjustable. With the sodium molten, cap screws covering the four bolts E are removed. The bolts E are withdrawn until the sockets F fit snugly against the end plate. The bolts E are then unscrewed and replaced with bolts of a different length. These are pushed back in and the cap screws refitted. This operation has been performed several times, and the average leakage is not more than 200 g. The system is topped up through the port A after this operation.

At present the instrumentation consists of two search coils, G, and a laboratory-made photo-electric torque meter through which the cylinder's basic rotation is driven. The search coil signal is brought out of the container and off the rotating table through copper slip rings with copper–carbon brushes. By adding or bucking the signals from the two coils one can cancel odd or even harmonics.

The torque-meter consists of two slotted wheels connected by a torsion bar. A light is passed through the pair into a photosensitive resistor and the change in resistance is measured. The slots are arranged such that no light can pass when the torsion bar is untwisted. Different ranges of torque can be investigated by using different torsion bars. Only static calibration of this device has been possible and this is not very accurate. However, for the work done to date only relative torque has been important; the air drag on the container swamps any signal that would be obtained in a range accessible by linear theory.

There is also a Bell Model 620 Gaussmeter in the laboratory with which one can investigate stray fields. This has not proved useful to date. In addition a strobotach with a photopickoff device is available, allowing one to compare the phase of the search coil signal with the actual position of the container.

The use of this experiment to clarify the theory developed in the first half of the paper is just barely possible. The dimensionless numbers E, E_m and C^2 are given by

$$E = 1{\cdot}1 \times 10^{-7},$$

$$E_m = 1{\cdot}3 \times 10^{-2},$$

$$C^2 = 1{\cdot}956 \times 10^{-6} I^2,$$

where I is the field coil current in amperes. The maximum I for which measurements have been made is 27 amperes. This gives $C^2 \sim 1{\cdot}5 \times 10^{-3}$ and $C^3 \sim 6 \times 10^{-5}$. Thus if $f = 0$, the maximum precession rate according to (5.9) is 0·2 rev/min. $E^{\frac{3}{4}} \sim 8 \times 10^{-6}$, giving a maximum precession rate of 0·03 rev/min. The transmission was not sufficiently sensitive to attain such low precession rates. The best that was attained was a precession rate of 0·133 rev/min.

To determine f absolutely one must be able to machine to an accuracy of 1 part in 10^4. The laboratory device was not built to such a tolerance, and even

were such tolerances attainable, centripetal deformations are of this order. Thus one cannot obtain f *a priori*. However, f controls both the amplitude and the shape of the curve of $A\epsilon_1$ *vs.* C^2, so that if one can find a single f which matches both, one can look at the data in the light of (5.8) and see if the f chosen is reasonable in that context.

The sign of f is critical. The secondary resonance phenomenon described following equation (5·6) is possible only for $f > 0$. Figure 2 shows $A\epsilon_1/R_p$ as a function of B using the values given above, for $f = 0, \pm 6 \times 10^{-3}$. The difference among the curves is striking.

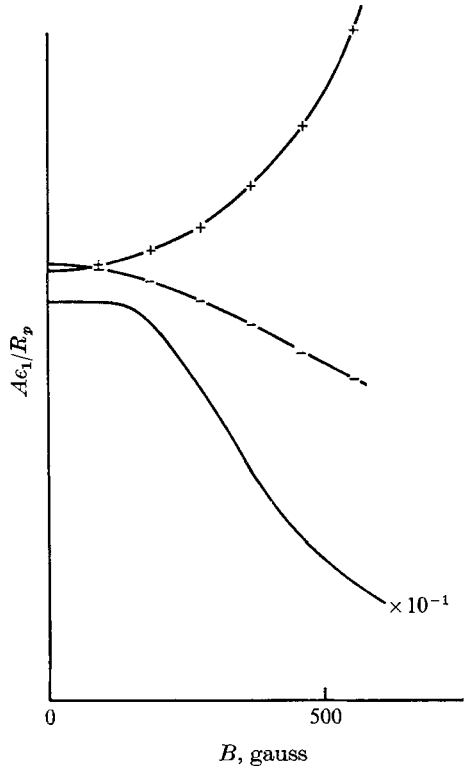

FIGURE 2. Response *vs.* applied magnetic field for $f = 0$ (solid line). $f = 6 \times 10^{-3}$ (pluses) and $f = -6 \times 10^{-3}$ (minuses). The $f = 0$ curve is reduced by a factor of 10.

One measures the electric field induced in the two search coils. This is proportional to $A\epsilon_1$. For a fixed rotation rate, this quantity, divided by the precession rate, is a function of the applied current I only. One can then build up a set of data by running the experiment at different precession rates and plotting the signal divided by the precession rate as a function of the current.

Misalignment of the main coil produces a signal of the same type as the theoretical response, but this signal is independent of precession rate. The coil is not securely attached to the rotating table and the misalignment can change from run to run, introducing large error bars on the data. These errors can be reduced drastically by accepting only the intersection of the various points at a given current strength.

A consistent picture of this kind can only be obtained by discarding all data with precession rates greater than or equal to 0·194 rev/min. There remain 31 points taken at 5 precession rates between 0·133 and 0·182 rev/min.

The data are expressed in terms of the peak-to-peak output voltage of the search coil-filter system, times the quarter period of precession in seconds, divided by the field coil current in amps. Denoting this quantity by $\mathscr{E}$, one has

$$\mathscr{E} = \frac{23e}{4\Omega}\left|\frac{\partial}{\partial\phi}\mathbf{h}.\hat{\mathbf{z}}\right|, \tag{6.1}$$

where e is the output of the search coils per unit magnetic field in volts/gauss, and the field coil produces 23 gauss/amp at the end plates. The number e is a function of the apparatus, and $|\partial\mathbf{h}.\hat{\mathbf{z}}/\partial\phi|$ is a function of the theory.

For the singly-periodic response

$$\left|\frac{\partial}{\partial\phi}\mathbf{h}.\hat{\mathbf{z}}\right| = |\epsilon_1 h_{1z} + \epsilon_2 \tilde{h}_{2z} + \ldots|$$

and $\tilde{h}_{2z}$ must be included to give a correct result. This is because that efflux is $O(E_m^{\frac{1}{2}})$ and $E_m^{\frac{1}{2}} = 0{\cdot}114$ is not negligible compared to 1 for the experiment. The quantity h_{2z} can be obtained from equation (5.8) by replacing δ_1 by $L_1\delta_1$, δ_2 by $L_2\delta_2$, δ_3 by $L_3\delta_3$ and δ_4 by $L_4\delta_4$. After manipulation one can write

$$\tilde{h}_{2z} \approx \frac{k^2}{6\sqrt{3}}\left(\frac{E}{E_m}\right)^{\frac{1}{2}}(3\sqrt{3}-i)\,V_1^b + \frac{1}{\sqrt{2}}\sqrt{E_m}(1-i)\,\Phi^b_{,zz}. \tag{6·2}$$

$(E/E_m)^{\frac{1}{2}} = 0{\cdot}0029$, and so only the second term is important. The singly periodic magnetic field is then

$$\epsilon h_{1z} + \epsilon_2 \tilde{h}_{2z} = -Re\{\tfrac{1}{4}\pi^2[1-\sqrt{\tfrac{3}{2}}\,\tfrac{1}{2}\pi\sqrt{E_m}(1-i)]\,A\epsilon_1 J_1(\tfrac{1}{2}\sqrt{3\pi}\,\varpi)\,e^{i\phi}\}. \tag{6.3}$$

Substituting the dimensionless numbers into (5.7) gives $A\epsilon_1$

$$A\epsilon_1 = \frac{5{\cdot}27R_p}{4{\cdot}90f - 1{\cdot}85\times10^{-5}I^2 - 2{\cdot}43\times10^{-4} + 3{\cdot}21i\times10^{-3}}. \tag{6.4}$$

Each search coil consists of 24,000 turns wound with an inside radius of 0·85 cm and an outside radius of 2·15 cm. At 60 Hz it produces an output of 0·623 V/G. The measurement is of the peak-to-peak signal of two such coils, introducing a factor of four. A filter used to reduce noise and higher harmonics reduces the signal introducing a factor of 0·097. Thus $e = 2{\cdot}51$ V/G $\pm$ 5 %. At the location of the search coils $J_1(k\varpi)_{,} = 0{\cdot}558$, is a maximum. Combining all the parameters gives

$$\mathscr{E} = \frac{0{\cdot}135}{\{[4{\cdot}90f - 1{\cdot}85\times10^{-5}I^2 - 7{\cdot}43\times10^{-4}]^2 - 1{\cdot}03\times10^{-5}\}^{\frac{1}{2}}} \pm 5\,\%. \tag{6.5}$$

Figure 3 shows a synthesis of the 31 data points retained, and the curve of $\mathscr{E}$ *vs.* I for $f = 6\times10^{-3}$. Within the 5 % error introduced by uncertainties regarding calibration of the search coil-filter system agreement is demonstrated.

The theoretical response as given includes the limitation of the resonance by viscous efflux from Ekman layers on the boundaries, mechanical departures from resonance, the change in the correct resonant length caused by the

magnetic field, and the magnetic efflux from magnetic Ekman layers. All of these phenomena are necessary to produce the theoretical curve of figure 3. The non-linear results follow.

In the purely hydrodynamic case the first departure from the steady-state flow given by the linear theory is a set of vortices which are generated near the axis of the flow, ejected to some two thirds of the radius where they remain for many rotation periods before collapsing again to the centre. These have been observed in both resonant and non-resonant containers. The axis of no velocity pitches about. From one to four of these vortices can exist at once.

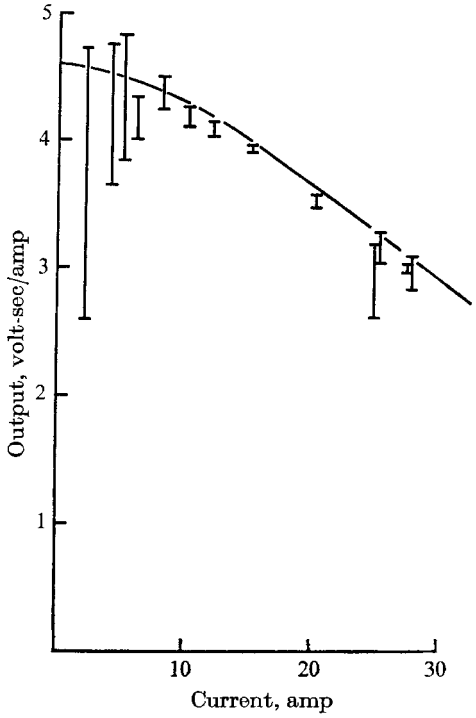

FIGURE 3. Field parameter *vs.* applied field current. Theory and experiment. The working fluid is sodium and the rotation rate is 3600 rev/min.

In the corresponding hydromagnetic case time-dependence of the search coil signal is observed. A useful analysis of this time-dependence has not yet been made because the problem of time-dependent noise has not yet been resolved. This appears to be a fruitful path for inquiry, however, especially in view of the complete lack of understanding of the hydrodynamic vortices.

At higher precession rates the non-resonant hydrodynamic cylinder exhibits a hysteresis behaviour in its torque curve. This is felt to be similar to the same phenomenon reported for sufficiently oblate spheroids by Malkus (1968). A tentative explanation for cylinders in terms of a subtle resonance phenomenon has been put forward by Gans (1969). Malkus (1968) suggests that this phenomenon may be a promising lead toward uncovering a dynamo mechanism.

Figure 4 shows the torque *vs.* precession rate curves for water in the device described above at 3600 rev/min for $L/D = 1$ (resonant) and $L/D = 0{\cdot}9$ (non-resonant). The torque scale is arbitrary. The distinction between the non-

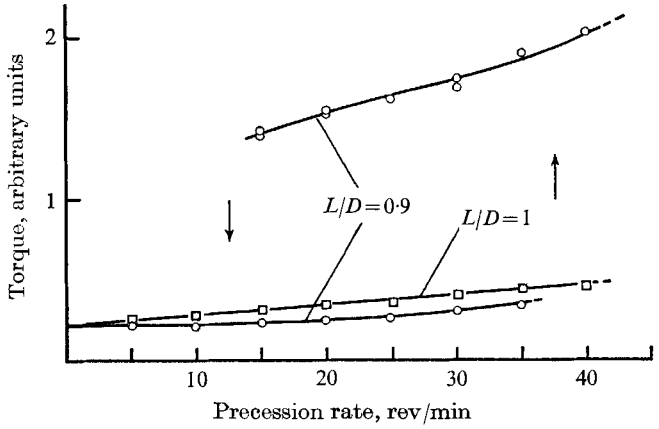

FIGURE 4. Torque *vs.* precession rate at $L/D = 1$ and $L/D = 0{\cdot}9$. The working fluid is water and the rotation rate 3600 rev/min.

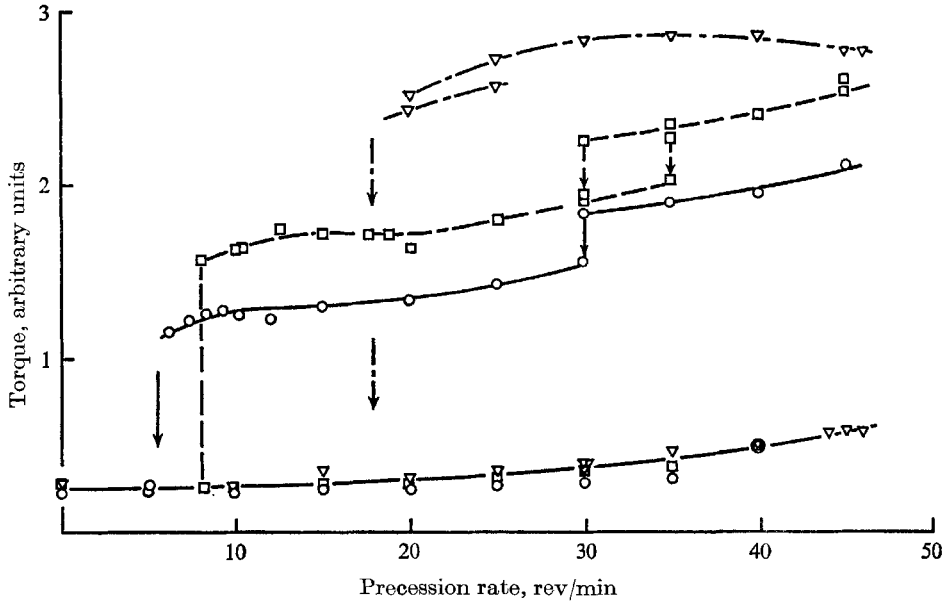

FIGURE 5. Torque *vs.* precession rate at $L/D = 0{\cdot}9$. The working fluid is sodium and the rotation rate is 3600 rev/min. The curves represent constraining field of: ——, 0 gauss; – – – –, 230 gauss; —·—, 460 gauss.

resonant and resonant curves is clear. Figure 5 shows the same curves in sodium constrained by 0, 230, and 460 G fields with $L/D = 0{\cdot}9$. For this run the rotating pressure union through which the nitrogen is introduced failed so there was a

vacuum core in the test section. This is not felt to be important for these torque curves.

At the point of transition the magnetic field measured by the search coils increased dramatically, jumping by about a factor of three. This amplification persisted when no field was applied and only the ambient field in the room was available.

The upward transition point at 230 and 460 G was beyond the capacity of the apparatus and transition was forced by removing the field and then the torque was measured by turning the field back on. This is a secondary test of the stability of the upper branch of the torque curve. At no time did addition of the field force it down to its pretransition height.

A secondary downward transition structure in the upper branch of the torque curve in the 0 and 230 G cases is a new feature of the conducting fluid. Such structure has not appeared in any of the hydrodynamic torque curves generated when the original hysteresis phenomenon was discovered. Unfortunately calibration problems prevent direct comparison of figures 4 and 5, so one cannot tell which, if either, of the torque domains corresponds to the hydrodynamic domain. It is also clear that the addition of a magnetic field moves the up and down transition points to higher precession rates. This can be qualitatively understood in terms of a general depressing effect of the field on the hydrodynamic response of precession.

This work is based on a dissertation submitted to the Department of Geology at the University of California, Los Angeles. Thanks are due especially to my chairman, Prof. W. V. R. Malkus, and to Mr Paul Cox, who built the apparatus described above almost from scratch, and to Prof. F. H. Busse, who critically reviewed the manuscript. Support from the National Science Foundation under grant GA-849, and from the National Aeronautics and Space Administration under grant NGL-05-002-003 is gratefully acknowledged.

Appendix. The free modes

The free modes of the system are given by the solutions of the dissipation-free version of equations (3.1) for arbitrary s and m. The general analogue of the eigenvalue problem (3.3) is

$$\left.\begin{gathered}\left\{\Delta-\frac{4}{\lambda^2}\frac{\partial^2}{\partial z^2}\right\}V=0;\\ \left\{2m+\lambda\frac{\partial}{\partial\varpi}\right\}V=0 \quad \text{on} \quad \varpi=1,\\ \frac{\partial V}{\partial z}=0 \quad \text{on} \quad z=\pm L/D.\end{gathered}\right\} \tag{A 1}$$

Here $\lambda = s+m-\alpha^2C^2(s+m)^{-1}$, and the eigenfunctions are

$$V = J_m(k_{mn}\varpi)\sin\alpha_n z\exp\left[i(m\phi+s_{mn}t)\right]; \tag{A 2}$$

clearly $\alpha_n = \frac{1}{2}(2n+1)\pi D/L$. The remaining parameters s_{mn} and k_{mn} are determined from the pair

$$\left.\begin{aligned} k_{mn}^2 - \alpha_{mn}^2\left(\frac{4-\lambda_{mn}^2}{\lambda_{mn}^2}\right) &= 0, \\ 2mJ_m(k_{mn}) + k_{mn}\lambda_{mn}J'_m(k_{mn}) &= 0. \end{aligned}\right\} \tag{A 3}$$

One can solve the first of (A 3) formally for $s+m$, the frequency that an observer rotating with the container would see. The result, in terms of k_{mn}, is

$$\pm(s+m) = \frac{(2n+1)\pi D/L}{\sqrt{(4k_{mn}^2 + [(2n+1)\pi D/2L]^2)}}\left\{1 \pm \left[1 + \left(k_{mn}^2 + \left[\frac{2n+1}{2}\pi\frac{D}{L}\right]^2\right)C^2\right]^{\frac{1}{2}}\right\}. \tag{A 4}$$

For fixed n and m, there is an infinite set of k_{mn}, $\{k_{lmn}\}$, and corresponding to each there are four values of s_{lmn}, as the $\pm$ sign on the left-hand side of (A 4) is independent of that on the right. Thus modes go both east and west, and no simple selection rule has appeared, capable of rationalizing the observed westward drift of the earth's magnetic field in terms of hydromagnetic waves.

Analysis parallel to that used in § 4 gives the boundary layers for a general $s+m$ modes as:

$$\delta^2 = -\frac{1}{2}\left\{\frac{iE}{s+m\mp 2} - \frac{C^2}{(s+m)(s+m\mp 2)} + \frac{iE_m}{s+m}\right\}$$
$$(\pm)\frac{1}{2}\left[\left\{\frac{iE}{s+m\mp 2} - \frac{C^2}{(s+m)(s+m\mp 2)} + \frac{iE_m}{s+m}\right\}^2 + \frac{4EE_m}{(s+m)(s+m\mp 2)}\right]^{\frac{1}{2}},$$
$$\text{on} \quad z = \pm L/D,$$
$$\delta^2 = -\frac{i}{2}\frac{E+E_m}{s+m}(1+\epsilon_{mn})^{-1}(\pm)\left[-\frac{(E+E_m)^2}{(s+m)^2}(1+\epsilon_{mn})^{-2} + \frac{4EE_m}{(s+m)^2}(1+\epsilon_{mn})^{-1}\right]^{\frac{1}{2}}. \tag{A 5}$$

In the second formula

$$\epsilon_{mn} = \left[\frac{2n+1}{2}\pi\frac{D}{L}\frac{C}{s+m}\right]^2.$$

REFERENCES

Busse, F. 1968 *J. Fluid Mech.* **33**, 739.

Erdelyi, A., Magnus, W., Oberhettinger, F. & Tricomi, F. G. 1953 *Higher Transcendental Functions*. New York: McGraw-Hill.

Gans, R. F. 1969 *Fellowship Lectures*. Summer Study Program in Geophysical Fluid Dynamics: Woods Hole Oceanographic Institution, References no. 69-41.

Gans, R. F. 1970 *J. Fluid Mech.* **41**, 865.

Lowes, F. J. & Wilkinson, I. 1968 *Nature, Lond.* **219**, 717.

Malkus, W. V. R. 1968 *Science*, **160**, 259.